

# How far away is far enough for extracting numerical waveforms, and how much do they depend on the extraction method?

Enrique Pazos,<sup>1,2,3</sup> Ernst Nils Dorband,<sup>1,2</sup> Alessandro Nagar,<sup>4,5</sup>  
Carlos Palenzuela,<sup>1</sup> Erik Schnetter,<sup>2</sup> and Manuel Tiglio<sup>1,2</sup>

<sup>1</sup>*Department of Physics and Astronomy, 202 Nicholson Hall,  
Louisiana State University, Baton Rouge, LA 70803, USA*

<sup>2</sup>*Center for Computation & Technology, 216 Johnston Hall,  
Louisiana State University, Baton Rouge, LA 70803, USA*

<sup>3</sup>*Departamento de Matemática, Universidad de San Carlos de Guatemala,  
Edificio T4, Facultad de Ingeniería, Ciudad Universitaria Z. 12, Guatemala*

<sup>4</sup>*Dipartimento di Fisica, Politecnico di Torino, Corso Duca Degli Abruzzi 24, 10129 Torino, Italy*

<sup>5</sup>*INFN, sez. di Torino, Via P. Giuria 1, Torino, Italy*

(Dated: December 22, 2006)

We present a method for extracting gravitational waves from numerical spacetimes which generalizes and refines one of the standard methods based on the Regge–Wheeler–Zerilli perturbation formalism. At the analytical level, this generalization allows a much more general class of slicing conditions for the background geometry, and is thus not restricted to Schwarzschild-like coordinates. At the numerical level, our approach uses high order multi-block methods, which improve both the accuracy of our simulations and of our extraction procedure. In particular, the latter is simplified since there is no need for interpolation, and we can afford to extract accurate waves at large radii with only little additional computational effort. We then present fully nonlinear three-dimensional numerical evolutions of a distorted Schwarzschild black hole in Kerr–Schild coordinates with an odd parity perturbation and analyze the improvement we gain from our generalized wave extraction, comparing our new method to the standard one. We do so by comparing the extracted waves with one-dimensional high resolution solutions of the corresponding generalized Regge–Wheeler equation.

We find that, even with observers as far out as  $R = 80 M$ —which is larger than what is commonly used in state-of-the-art simulations—the assumption in the standard method that the background is close to having Schwarzschild-like coordinates increases the error in the extracted waveforms considerably. Even for our coarsest resolutions, our new method decreases the error by between one and two orders of magnitudes. Furthermore, we explicitly see that the errors in the extracted waveforms obtained by the standard method do not converge to zero with increasing resolution. That is, these errors are dominated by the extraction method itself and not by the accuracy of our simulations. We analyze in detail the quasinormal frequencies of the extracted waves, using both methods.

In a general scenario, for example a collision of compact objects, there is no precise definition of gravitational radiation at a finite distance, and gravitational wave extraction methods at such distances are thus inherently approximate. The results of this paper bring up the possibility that different choices in the wave extraction procedure at a fixed and finite distance may result in relative differences in the waveforms which are actually larger than the numerical errors in the solution.

PACS numbers: 04.25.Dm, 04.25.Nx, 04.70.Bw

## I. INTRODUCTION

One of the goals of numerical solutions of Einstein’s equations is usually the prediction and analysis of the gravitational radiation emitted in some physical process. There are many methods for computing, or *extracting*, gravitational waves from a numerical spacetime. They can be broadly divided into two groups, depending on whether the solution includes null infinity (or a portion of it), or whether the computational domain is truncated at a hopefully large but finite distance from the source. In the first case, gravitational radiation can be defined and extracted in an unambiguous, rigorous way (see e.g. [1] and references therein, and [2]). In the second case, some approximation has to be made; not only at the level of the observer being in the radiation zone, but also

in the way the “gravitational radiation” is computed in terms of the spacetime metric. Due to the additional complexity of evolving Einstein’s equations all the way up to null infinity, currently most simulations actually truncate the computational domain by placing an artificial outer boundary at a finite distance. This paper deals with one particular approach to gravitational wave extraction from spacetimes within this second group.

In general, one expects the differences between the exact waveforms and those extracted at a finite distance to decay as the extraction radius increases. One natural question that arises is: for a given extraction method, how far away is far enough, so that the errors in the extracted waves are dominated by the accuracy of the simulations used to obtain the numerical spacetime, and not by the extraction mechanism itself? In this paper we address this question in detail in a very particular scenario,

but which might shed some light on the general case.

The main idea of extracting waves at a finite distance is to exploit the structure of an asymptotically flat spacetime. One reads off the quantities which are needed to compute the gravitational radiation from the numerically generated solution. The method which we consider in this paper is based on the well-known perturbations of the Schwarzschild spacetime. See e.g. [3, 4, 5, 6, 7, 8, 9, 10, 11, 12, 13, 14] for other approaches based on the Weyl scalar  $\Psi_4$ .

One possible approach is to assume that the full metric in the region of extraction can be considered as a perturbation of a flat spacetime, and to read off such perturbations from the numerical solution. This approach is justified by the fact that the leading order of the metric at large distances (in an expansion in powers of  $1/r$ ) is flat. If the waves are extracted at a large but finite distance from the source, it makes sense to try to decrease the errors of the approximation by further considering the next order in the expansion of the metric, which is described by the Schwarzschild solution. In doing so, the numerical metric is not considered anymore a perturbation of flat spacetime, but instead of the Schwarzschild geometry. One can consider even higher orders in this background identification, such as the spin contribution. However, an important fact to keep in mind is that all these methods should in principle give the same gravitational radiation as the radius of extraction increases. In other words, one should be able to compute the gravitational radiation through, for example, perturbations of a flat spacetime or the Schwarzschild metric, and the radiation should contain the information about the spacetime's non-zero mass and—if present—angular momentum when the observer is at large enough distances.

If only the first or the first two orders in the asymptotic expansion of the metric are kept when identifying this distant “background” geometry, then the framework for extracting gravitational radiation is that of perturbations of flat spacetime or of the Schwarzschild geometry, respectively. One can view the former as a subcase of the latter, so that from hereon we will just consider perturbations of the Schwarzschild spacetime. In this case, perturbations decouple into two separate sectors, which differ in the parity of the perturbations (odd or even). These two parity sectors are directly related to the real and imaginary parts of the Weyl scalar  $\Psi_4$  (see, for example, ref. [15]). Gauge invariant formalisms for such perturbations were developed by Regge and Wheeler [16] in the fifties for the odd-parity sector and by Zerilli [17] in the seventies for the even-parity sector.

The idea of using Regge–Wheeler–Zerilli perturbation theory to extract gravitational waves from numerical spacetimes is definitely not new. It goes back to pioneering work by Abrahams and Evans [18, 19, 20] (see also [21]) and it has been used extensively since the birth of numerical relativity (see [22] for a review). For example, the accuracy of simulations of distorted black holes was tested by comparing extracted waveforms against per-

turbative calculations [23, 24, 25, 26, 27], and often, also technical improvements (such as excision) were tested by studying their effects on waveforms [28, 29]. Recently, [30] reported Zerilli waveforms from unequal mass binary black hole inspirals. In hydrodynamical simulations, gravitational waves are often determined via the quadrupole formula, which usually gives more accurate information in these particular situations (unless a black hole is present), since the wave amplitude is typically very small and thus difficult to detect from the spacetime metric [31, 32, 33].

In this paper we present a generalization of this approach to gravitational wave extraction with two salient features. The first is at the level of the perturbation formalism itself: we use a generalization of the standard Regge–Wheeler–Zerilli (RWZ) formalism, which is not only gauge invariant, but also covariant [15, 34, 35, 36], in the sense that it is independent of the background coordinates. The standard RWZ formalism is gauge invariant only in the sense that the background metric is fixed to the Schwarzschild geometry *in Schwarzschild coordinates*, and the formalism is invariant with respect to infinitesimal, first order changes of coordinates, which keep the background coordinates *fixed*. However, in numerical simulations of Einstein's equations, the numerical spacetime might be close to the Schwarzschild geometry in certain situations (say, at large distances), but the metric does not need to be close to the Schwarzschild metric *in Schwarzschild coordinates*. In fact, when dealing with the black hole singularity through black hole excision, one uses coordinates that are well defined in a neighborhood of the horizon, and which are therefore clearly not of Schwarzschild type.

This first salient improvement (the use of a generalized formalism) is independent of the details of the numerical implementation. The second improvement is tied to our particular numerical approach, which uses high order methods (typically higher than four) for high accuracy, and uses multiple blocks with adapted grids, non-trivial topologies, and smooth boundaries. The use of high order methods for both the evolution of Einstein's equations and for the wave extraction procedure itself, combined with the use of shells of “spherical” patches or blocks, allows us to extract gravitational waves in a simple, fast, and accurate way. In particular, *we can keep both the angular and radial resolutions fixed* and place the outer boundaries at large distances, using considerably less computational resources than what would be needed with Cartesian grids, even when using mesh refinement. In addition, no interpolation to spheres is needed to extract waves on spherical shells.

For weak perturbations of a Schwarzschild black hole we can actually obtain the exact solution by evolving the generalized Regge–Wheeler equation. Since this is a wave equation in  $1 + 1$  dimensions, we can solve it with almost arbitrarily high accuracy. For all practical purposes, we consider it to be an exact solution, against which we can compare the extracted waveforms from our

three-dimensional evolutions. We evolve weak perturbations of a Schwarzschild black hole in Kerr–Schild coordinates, using the fully nonlinear Einstein equations. We find that the assumption in the standard method that the background is in Schwarzschild–like coordinates increases the error in the extracted waves (as compared to extracting with the correct background) by between one and two orders of magnitudes. This is true even with observers as far away as  $80 M$ , and even for the coarsest resolutions that we use. Furthermore, we explicitly see that the errors in the standard method do not converge to zero with increasing resolution at any fixed extraction radius, while they do with the generalized method. The errors only decrease (as  $1/r$ , as we discuss in sect. IV) as the observer radius is increased. That is, if one does not use the correct background coordinates, these errors are dominated by the extraction procedure and not by the accuracy of the simulations. We compare the quasinormal frequencies of the waves extracted the above methods against the results predicted by perturbation theory.

The organization of this paper is as follows. In sect. II we describe in a self-contained way the generalized perturbation formalism, restricted to the odd-parity sector (we will present a similar treatment for the even parity sector elsewhere), and our construction of the Regge–Wheeler function from a numerical spacetime. We also use the inverse problem (that is, the generation of a perturbed metric from any given Regge–Wheeler function) to construct initial data that automatically satisfies the Einstein constraints when linearized around the Schwarzschild spacetime, which does not necessarily need to be given in Schwarzschild coordinates. This is the data that we later evolve and use in our numerical tests.

In sect. III we briefly describe our numerical techniques, our formulation of Einstein’s equations, and our outer boundary conditions. Finally, we present our numerical results in sect. IV. We first show that our extracted covariant and gauge invariant Regge–Wheeler function coincides very well with the expected one from perturbation theory (which we obtain by solving the 1+1 generalized Regge–Wheeler equation) when we use the generalized formalism to identify the background correctly. After that, we compare our covariant and gauge invariant extracted waveforms with those obtained by the traditional approach, which assumes that the background is either the Minkowski spacetime in Minkowski coordinates, or the Schwarzschild spacetime in Schwarzschild coordinates. In sect. V we discuss these results in the broader context of gravitational wave extraction for generic spacetimes.

For completeness, in Appendix A we describe in detail our conventions for tensor spherical harmonics decompositions.

## II. ODD-PARITY PERTURBATIONS OF SCHWARZSCHILD AND WAVE EXTRACTION

This section summarizes the results of the generalized formalism relevant for this paper. We closely follow the notation and presentation of ref. [15].

### A. The background metric and tensor spherical decomposition of the perturbations

The generalized formalism assumes that the total metric can be written as

$$g_{\mu\nu}^{\text{tot}} = g_{\mu\nu} + \delta g_{\mu\nu} \quad (1)$$

where  $g_{\mu\nu}$  describes the Schwarzschild geometry and  $\delta g_{\mu\nu}$  is, in some sense, a “small” correction. Further, it is assumed that the four-dimensional manifold can be decomposed as the product of a two-dimensional manifold  $\mathcal{M}$  parametrized with coordinates  $x^a$  ( $a = 0, 1$ ) and a unit 2-sphere  $S^2$  with coordinates  $x^A$  ( $A = 2, 3$ ), such that the background Schwarzschild metric takes the form

$$ds^2 = \tilde{g}_{ab}(t, r) dx^a dx^b + f^2(t, r) \hat{g}_{AB} dx^A dx^B. \quad (2)$$

Capital Latin indices refer to angular coordinates  $(\theta, \phi)$  on  $S^2$ , while lower-case ones refer to the  $(t, r)$  coordinates. Here  $\hat{g}_{AB}$  is the standard metric on the unit sphere,  $\tilde{g}_{ab}$  denotes the metric tensor on the manifold  $\mathcal{M}$ , and  $f^2$  is a positive function. If one uses an areal radius coordinate, then  $f = r$ , but we do not make such an assumption. Actually, as we discuss below, the fact that our formalism is general enough to allow for  $f = f(t, r)$  has practical advantages in the wave extraction procedure. For simplicity, the metric on the unit 2-sphere  $S^2$  is assumed to be in standard coordinates:  $\hat{g}_{AB} = \text{diag}(1, \sin^2 \theta)$ . Summarizing, we are assuming that the background Schwarzschild metric is given in a coordinate system in which there is no angular shift, but there can be a radial shift. Note that there is no assumption about the shift in the perturbation.

From a numerical relativity point of view, it is usually convenient to deal with the variables that appear in the 3+1 split of spacetime. To this end, we follow the notation of ref. [15] and explicitly expand the components of the background Schwarzschild metric as

$$ds^2 = (-\alpha^2 + \gamma^2 \beta^2) dt^2 + 2\gamma^2 \beta dt dr + \gamma^2 dr^2 + f^2(d\theta^2 + \sin^2 \theta d\phi^2) \quad (3)$$

where  $\alpha$  and  $\beta \equiv \beta^r$  are the background lapse and radial shift vector, respectively, and  $\gamma^2 \equiv \tilde{g}_{rr}$ . Since the background is spherically symmetric, it is convenient to expand the perturbations in spherical harmonics,

$$\delta g_{\mu\nu} = \sum_{\ell=1}^{\infty} \sum_{m=-\ell}^{\ell} \delta g_{\mu\nu}^{(\ell, m)}. \quad (4)$$

In the odd-parity sector there is no perturbation for  $\ell = 0$ . The dipole term,  $\ell = 1$ , corresponds to the linearization of the Kerr metric using the angular momentum of the spacetime as a parameter. Thus, for gravitational wave extraction we only need to consider perturbations with  $\ell \geq 2$ . These quantities can be parametrized according to

$$\begin{aligned}\delta\beta_A^{(\ell,m)} &= b^{(\ell,m)} S_A^{(\ell,m)} \\ \delta g_{rA}^{(\ell,m)} &= h_1^{(\ell,m)} S_A^{(\ell,m)} \\ \delta g_{AB}^{(\ell,m)} &= h_2^{(\ell,m)} S_{AB}^{(\ell,m)} \\ \delta K_{rA}^{(\ell,m)} &= \pi_1^{(\ell,m)} S_A^{(\ell,m)} \\ \delta K_{AB}^{(\ell,m)} &= \pi_2^{(\ell,m)} S_{AB}^{(\ell,m)}.\end{aligned}\quad (5)$$

Using the covariant derivative  $\hat{\nabla}_A$  compatible with the metric  $\hat{g}_{AB}$  on the unit sphere  $S^2$  and its associated Levi-Civita tensor  $\hat{\epsilon}_{AB}$  (with non-vanishing components  $\hat{\epsilon}_{\theta\phi} = \sin\theta = -\hat{\epsilon}_{\phi\theta}$ ), we define  $S_A = \hat{\epsilon}_A^B \hat{\nabla}_B Y$  (the first index in  $\hat{\epsilon}$  raised with the inverse of  $\hat{g}$ ) and  $S_{AB} = \hat{\nabla}_{(A} S_{B)}$ . Here,  $Y \equiv Y^{(\ell,m)}$  are the standard spherical harmonics. The quantities  $S_A$  and  $S_{AB}$  form a basis on  $S^2$  for odd-parity vector and symmetric tensor fields, respectively. For completeness, we give a detailed and self-consistent description of how to use these to decompose vectors and tensors into spherical harmonics in Appendix A.

From now on, we suppress the superindices  $(\ell, m)$  and the sum over them, since modes belonging to different pairs of  $(\ell, m)$  decouple from each other in the perturbation formalism.

## B. Extraction of the Regge–Wheeler function from a given geometry

To define the background metric, we extract the  $\ell = 0$  component (that is, the spherically symmetric part) of the numerical solution  $g_{\mu\nu}^{\text{tot}}$ . This is done by decomposing the metric  $\tilde{g}_{ab}$  of the two-dimensional manifold  $\mathcal{M}$  into spherical harmonics. These metric components behave like scalars under a rotation of coordinates. Thus, the background metric is computed as

$$\tilde{g}_{ab} = \frac{1}{4\pi} \int g_{ab}^{\text{tot}} d\Omega, \quad (6)$$

where  $d\Omega$  is the standard area element on  $S^2$ . The function  $f$  can be computed through  $f = \sqrt{A/4\pi}$ , with

$$A = \int \sqrt{\hat{g}} d\theta d\phi, \quad (7)$$

where the integration is performed over the extraction 2-sphere, and  $\hat{g}$  is the determinant of  $\hat{g}_{AB}$ .

Similarly, we compute the perturbed quantities by extracting the  $\ell \geq 2$  components of the numerical metric  $g_{\mu\nu}^{\text{tot}}$ , in the way explained in Appendix A.

Once we have obtained the multipoles  $b, h_1, h_2, \pi_1, \pi_2$  defined above in eq. (5) and the background quantities  $f, \alpha, \gamma, \beta$  defined in eq. (3), we can find the generalized gauge-invariant Regge–Wheeler (RW) function  $\Phi_{RW}$ . It is given by [15]

$$\Phi_{RW} = \frac{2f}{\lambda\alpha\gamma} \left( \alpha\pi_1 - \frac{\partial_0 f}{f} h_1 \right) \quad (8)$$

where  $\partial_0 \equiv \partial_t - \beta\partial_r$  and  $\lambda = (\ell-1)(\ell+2)$ . Notice from eq. (8) that the *only* multipole components appearing in the RW function  $\Phi_{RW}$  are  $h_1$  and  $\pi_1$ , so that there is no need to compute the others.

Previous approaches to compute waveforms with the standard RWZ formalism have typically been considerably more involved than what we have just described. We briefly sketch the standard approach here. Einstein’s equations are usually solved using Cartesian coordinates on a Cartesian grid. The numerically obtained metric is first transformed to polar-spherical coordinates. Performing the multipole decomposition on a given coordinate sphere requires a numerical integration over that sphere, which in turn requires interpolating the metric to the spherical surface, which does not coincide with the grid points of the Cartesian grid. Integrating over the sphere also allows computing the areal radius and its radial derivatives. These quantities are then used to transform the metric in a second step to its final form in “Schwarzschild-like” coordinates. This is done by first changing from the coordinate radius to an areal radius (which requires the numerically calculated radial derivatives), and then identifying the  $(t, r)$  components of the metric in this new coordinate system, which is assumed to be a perturbation of the Schwarzschild metric in Schwarzschild coordinates. With all this in place, the waveforms are then computed using standard RWZ formulae.

In our case, the multi-block grid structure naturally allows for spherical surfaces. Hence, no interpolation is required. The generalized perturbation formalism allows us to compute the RW function  $\Phi_{RW}$  without transforming the metric to Schwarzschild coordinates. In particular, the transformation to an areal radial coordinate is not required at all. Thus, our extraction procedure amounts simply to numerical integrations at a given value of the radial coordinate to compute the multipoles, and then using eq. (8) to compute the RW function. An additional improvement is that our high order accurate derivative operators are naturally associated with a high order accurate discrete norm, leading to an integration procedure which has the same accuracy as our derivative operators.

## C. (Re)construction of the metric from the Regge–Wheeler function

It can be seen (see, for example, ref. [15] for more details of what follows) that for any slicing of Schwarzschild of the type given in eqs. (2) or (3), that we can construct

a perturbed four-metric from the RW potential. The perturbation coefficients of the linearized metric, as defined

in eq. (1), become

$$\delta g_{r\theta} = \left[ \frac{\gamma}{\alpha} \left( -f\dot{\Phi}_{RW} + \beta f\Phi'_{RW} + \Phi_{RW}(\beta f' - \dot{f}) \right) + \frac{fk' - 2kf'}{f} \right] \frac{Y_\phi}{\sin \theta} \quad (9)$$

$$\delta g_{r\phi} = - \left[ \frac{\gamma}{\alpha} \left( -f\dot{\Phi}_{RW} + \beta f\Phi'_{RW} + \Phi_{RW}(\beta f' - \dot{f}) \right) + \frac{fk' - 2kf'}{f} \right] \sin \theta Y_\theta \quad (10)$$

$$\delta g_{\theta\theta} = \frac{2k}{\sin^2 \theta} [-\cos \theta Y_\phi + \sin \theta Y_{\theta\phi}] \quad (11)$$

$$\delta g_{\phi\phi} = k [\cos \theta Y_\theta + \sin^{-1} \theta Y_{\phi\phi} - \sin \theta Y_{\theta\theta}] \quad (12)$$

$$\delta g_{\theta t} = \left[ \frac{1}{\gamma\alpha} \left( -\gamma^2 \beta f\dot{\Phi}_{RW} + f(\gamma^2 \beta^2 - \alpha^2) \Phi'_{RW} + (-\alpha^2 f' - \dot{f}\beta\gamma^2 + f'\gamma^2 \beta^2) \Phi_{RW} \right) + \frac{f\dot{k} - 2k\dot{f}}{f} \right] \frac{Y_\phi}{\sin \theta} \quad (13)$$

$$\delta g_{\phi\phi} = 2k [\cos \theta Y_\phi - \sin \theta Y_{\theta\phi}] \quad (14)$$

$$\delta g_{\phi t} = - \left[ \frac{1}{\gamma\alpha} \left( -\gamma^2 \beta f\dot{\Phi}_{RW} + f(\gamma^2 \beta^2 - \alpha^2) \Phi'_{RW} + (-\alpha^2 f' - \dot{f}\beta\gamma^2 + f'\gamma^2 \beta^2) \Phi_{RW} \right) + \frac{f\dot{k} - 2k\dot{f}}{f} \right] \sin \theta Y_\theta \quad (15)$$

Here dots and primes denote derivatives with respect to time and radius, respectively. It is  $Y_\phi = \partial_\phi Y$ ,  $Y_\theta = \partial_\theta Y$ , and as before we are skipping the  $(\ell, m)$  superindices.  $\gamma$ ,  $\alpha$ ,  $\beta$ , and  $f$  are defined in eq. (3). It can be seen that the function  $k$  is a pure gauge term and completely

arbitrary; in particular, we can make it vanish (resulting in the so called Regge–Wheeler gauge) through a first order coordinate transformation.

The generalized RW equation is

$$\ddot{\Phi}_{RW} = c_1 \dot{\Phi}'_{RW} + c_2 \Phi''_{RW} + c_3 \dot{\Phi}_{RW} + c_4 \Phi'_{RW} - \alpha^2 V \Phi_{RW} \quad (16)$$

with the coefficients  $c_i$  and the potential  $V$  given by

$$c_1 = 2\beta \quad (17)$$

$$c_2 = \frac{(\alpha^2 - \gamma^2 \beta^2)}{\gamma^2} \quad (18)$$

$$c_3 = \frac{(\gamma\dot{\alpha} - \gamma\beta\alpha' + \alpha\beta\gamma' - \alpha\dot{\gamma} + \gamma\alpha\beta')}{\gamma\alpha} \quad (19)$$

$$c_4 = \frac{1}{\gamma^3 \alpha} \left( -\gamma^3 \beta \dot{\alpha} - \alpha^3 \gamma' + \gamma^3 \beta^2 \alpha' - 2\gamma^3 \alpha \beta \beta' + \gamma^3 \alpha \dot{\beta} + \gamma^2 \alpha \beta \dot{\gamma} + \gamma \alpha^2 \alpha' - \gamma^2 \alpha \beta^2 \gamma' \right) \quad (20)$$

$$V = \frac{1}{f^2} \left[ \ell(\ell+1) - \frac{6M}{f} \right]. \quad (21)$$

When the background metric is Schwarzschild in Schwarzschild coordinates, this generalized RW equation coincides of course with the standard equation. Below, in sect. IV, we use high-resolution solutions of this generalized 1 + 1 equation as “exact” solutions, against which we compare the extracted RW function from our three-dimensional distorted black hole simulations.

### III. FORMULATION OF THE EQUATIONS, BOUNDARY CONDITIONS, INITIAL DATA, AND NUMERICAL METHODS

#### A. Evolution equations

The numerical simulations shown below were performed by evolving a first order symmetric hyperbolic



reduction of the Generalized Harmonic formalism, as constructed in ref. [37]. In this formulation, the coordinates  $x^\mu$  are chosen to satisfy the (generalized) harmonic condition<sup>1</sup> [38]

$$\nabla^\sigma \nabla_\sigma x^{(\mu)} = H^{(\mu)}(t, x^i), \quad (22)$$

where the gauge source functions  $H^{(\mu)}(t, x^i)$  are freely specifiable functions of the spacetime coordinates, and  $\nabla_\mu$  is the covariant derivative associated with  $g_{\mu\nu}$ . Here we omit the label “tot” from the metric (1) for the sake of simplicity. The reduction from second to first order is achieved by introducing the first derivatives of the metric  $g_{\mu\nu}$  as independent quantities. Following ref. [37], we introduce the quantities

$$Q_{\mu\nu} = -n^\sigma \partial_\sigma g_{\mu\nu} \quad (23)$$

$$D_{i\mu\nu} = \partial_i g_{\mu\nu}, \quad (24)$$

where  $n_\mu = -\alpha \nabla_\mu t$  is the (future directed) timelike unit normal vector to the hypersurface  $t = x^0 = \text{const.}$  Thus, the evolution equations for  $Q_{\mu\nu}$  are given by the Generalized Harmonic formalism, while the evolution equations for  $D_{i\mu\nu}$  are obtained by applying a time derivative to their definition (24) and commuting the temporal and spatial derivatives. Finally, the metric  $g_{\mu\nu}$  is evolved using the definition of  $Q_{\mu\nu}$ , eq. (23). In addition, in the spirit of refs. [39, 40], the constraints of this system are added to the evolution equations in such a way that the physical solutions (i.e., those satisfying the constraints) are an attractor in certain spacetimes. In those situations, small constraint violations will be damped during the evolution. The whole construction of this formulation of the equations is described in detail in [37].

The standard 3 + 1 components of the metric (i.e., the lapse function  $\alpha$ , the shift  $\beta^i$ , and the intrinsic metric  $\gamma_{ij}$ ) can be obtained via the relations

$$\alpha^2 = -1/g^{tt} \quad (25)$$

$$\beta_i = g_{ti} \quad (26)$$

$$\gamma_{ij} = g_{ij}. \quad (27)$$

The extrinsic curvature is defined in terms of the intrinsic metric as

$$K_{ij} = \frac{1}{2\alpha}(\partial_t - \mathcal{L}_\beta)\gamma_{ij}. \quad (28)$$

It can be recovered from the fields  $Q_{\mu\nu}$ ,  $D_{i\mu\nu}$  via

$$\begin{aligned} -2\alpha K_{ij} &= \alpha Q_{ij} + D_{itj} + D_{jti} \\ &\quad - \gamma^{km} \beta_m (D_{ijk} + D_{jik}). \end{aligned} \quad (29)$$

<sup>1</sup> In this subsection we use the Latin indices  $i, j, k, \dots$  to denote three-dimensional spatial quantities, while Greek indices continue to represent the four-dimensional ones.

In our simulations below we also monitor the Hamiltonian and momentum ADM constraints, namely,

$$\mathcal{H} = \frac{1}{2} \left( {}^{(3)}R - K_{ij}K_{ij} + (trK)^2 \right) \quad (30)$$

$$\mathcal{M}_i = \nabla_k (K_i^k - \delta_i^k trK), \quad (31)$$

where  ${}^{(3)}R$  is the Ricci scalar associated to the three-dimensional space-like metric  $\gamma_{ij}$ .

We impose maximally dissipative boundary conditions at the outer boundary. While these conditions guarantee well-posedness of the associated initial value problem, and thus numerical stability with our particular discretization, they are physically incorrect in the sense that they do not include back-scattered radiation from outside the simulation domain. For that reason, in the simulations shown below we place the outer boundary at large enough distances so that our extracted waves are causally disconnected from boundary effects.

## B. Multi-block approach

We use multi-block (also called multi-patch or multi-domain) methods for our numerical calculations. These have several advantages over single-domain methods:

*Smooth boundaries.* They provide smooth outer and inner boundaries, which is in general required [41] for a well-posed initial boundary value problem.

*Constant resolution.* They allow us to use constant radial and angular resolutions. This is not possible with mesh refinement methods. The way in which mesh refinement is typically used leads to a decreasing radial resolution, which makes it difficult to extract accurate gravitational wave information in the wave zone of a binary black hole system. (See sect. V, where we list typical wave extraction radii and resolutions.)

*No time-stepping restrictions.* They do not lead to a deterioration of the CFL factor for co-rotating coordinates. (For example, [42] reports that the CFL factor had to be reduced on the outermost refinement levels. The same was done later in [43].)

*Adapted to symmetries.* They can be adapted to the symmetries of a system. Obviously, adapted coordinates can reduce the discretization error significantly. In our case, we use on each block one radial and two angular coordinates to model the geometry of a single black hole. For binary black hole systems, one can use blocks that are roughly spherical near the individual holes and far away in the wave zone, with a transition region in between. Fig. 5 in [44] shows a possible multi-block system for this.

*No coordinate singularities.* They have no coordinate singularities. Spherical or cylindrical coordinates have singularities on the  $z$  axis which may cause problems. An alternative approach which avoids these singularities would be to use a pseudo-spectral decomposition into spherical harmonics. This was used in [45] to evolve

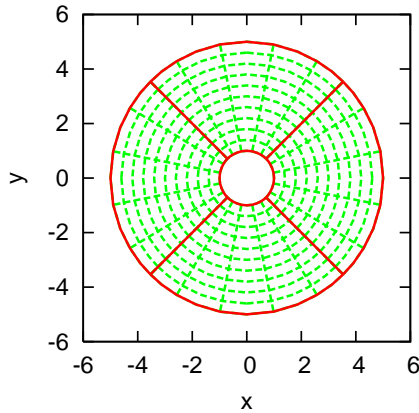


Figure 1: The equatorial plane of an example six-block geometry, cutting through four blocks. Note that the blocks do not overlap. All six blocks are made up identically. The outer and inner boundaries are smooth spheres. The outer boundary in our typical simulations is actually located much further out than shown here.

scalar fields on a Kerr background, in [46, 47] to evolve Einstein's, and in [48, 49, 50, 51, 52, 53] to set up initial data for various black hole and neutron star configurations.

Of course, using multiple blocks adds to the complexity of an implementation. However, the properties of multi-block systems for hyperbolic equations are by now well understood, and we describe our particular approach in [54] and [55], and in some detail in [44]. In this particular paper we use a *six-block system* to discretize the geometry of a single black hole, which is depicted in fig. 1. We use the same tensor basis on each block, namely a global three-dimensional Cartesian coordinate system. We found that this greatly simplifies the inter-block boundary conditions, since all components of tensorial quantities are then scalars with respect to the block-local coordinate systems.

We use the *penalty method* to enforce the inter-block boundary conditions. The penalty method for finite differences is described in [56, 57, 58], and we describe our approach and notation in [44, 54, 55]. In short, the penalty method works as follows. The individual blocks do not overlap, but they have their boundary points in common. The evolution equations are first discretized on each block independently using one-sided derivatives near the block boundaries. Then a correction term is added to the right hand side of the time derivative of each characteristic variable at the boundary points, penalising the difference between the left and right eigenmode values  $u^l$  and  $u^r$  on the boundary points:

$$\partial_t u^l \rightarrow \partial_t u^l + \frac{S^l}{h^l \sigma^l} (u^r - u^l) \quad (32)$$

$$\partial_t u^r \rightarrow \partial_t u^r + \frac{S^r}{h^r \sigma^r} (u^l - u^r). \quad (33)$$

Here  $h^l$  and  $h^r$  are the grid spacings on the two blocks,

which may be different. These penalty terms ensure continuity between the two blocks in the continuum limit and numerical stability in the semidiscrete case if the relevant parameters are appropriately chosen. The quantities  $\sigma^l$  and  $\sigma^r$  depend on the coefficients of the differencing operators that are used on the two blocks.<sup>2</sup> The parameters  $S^l$  and  $S^r$  determine how much (if any) dissipation is introduced across the block boundary. To ensure stability, they must be chosen in a very specific way depending on the characteristic speeds of the evolution system.

We have implemented this in the Cactus framework [62, 63], using the Carpet driver [64, 65] and the Cactus-Einstein toolkit [66].

### C. Initial data

If the RW function  $\Phi_{RW}$  satisfies the RW equation (16), then the perturbed metric constructed in sect. II C satisfies the linearized Einstein equations. Furthermore, it can be explicitly shown that this metric initially satisfies the linearized constraints around the Schwarzschild geometry for *any* initial values  $\Phi_{RW}(t = 0, r)$  and  $\dot{\Phi}_{RW}(t = 0, r)$ .<sup>3</sup> We take advantage of this property and construct initial data in a simple way as a test our new wave extraction method. For our simulations below, we use Kerr–Schild coordinates for the Schwarzschild background, and for the distortion we set  $\ell = 2$ ,  $m = 0$ , and choose

$$\begin{aligned} \Phi_{RW}(t = 0, r) &= 0, \\ \dot{\Phi}_{RW}(t = 0, r) &= A e^{(r-r_0)^2/\sigma^2} \end{aligned} \quad (34)$$

with parameters  $r_0$  and  $\sigma$ . This corresponds to a Gaussian pulse of width  $\sigma$  centered at  $r = r_0$ .

If we assume that we can Taylor-expand (a suitable norm of) the discrete non-linear constraints in terms of the perturbation amplitude  $A$  for any fixed gridspacing  $h$ , we have

$$\begin{aligned} \mathcal{C}(A, h) &= \mathcal{C}(A, h)|_{A=0} \\ &+ A \left. \frac{\partial \mathcal{C}(A, h)}{\partial A} \right|_{A=0} \\ &+ \frac{A^2}{2} \left. \frac{\partial^2 \mathcal{C}(A, h)}{\partial A^2} \right|_{A=0} + \mathcal{O}(A^3). \end{aligned} \quad (35)$$

Since in the continuum the linearized constraints are satisfied, the first two terms in the above expansion vanish for  $h \rightarrow 0$ , but otherwise are of the order of the

<sup>2</sup> To be exact,  $\sigma^l$  and  $\sigma^r$  depend on the coefficients of the discrete norms that are used in the blocks, but the differencing operators and the norms are usually chosen together to satisfy *summation by parts*. See [59, 60, 61], and especially [55].

<sup>3</sup> When constructing initial data for the 3+1 quantities, one also needs to take time derivatives of the four-metric; where second time derivatives of  $\Phi_{RW}$  appear, we use the RW equation to trade these for space derivatives.

truncation error. For small enough  $A$  the first term (that is, the background contribution) dominates, and the term  $C(A, h)$  appears to be independent of  $A$ . For large enough  $A$ , on the other hand, the quadratic term in the expansion given by eq. (35) will dominate.

Fig. 2 presents numerical evidence that this expected behavior is indeed the case. We set up numerical data according to eq. (34), with perturbation amplitudes  $A$  between  $10^{-6}$  and  $10^{-1}$ . The radial domain extent is  $1.8 \leq r \leq 7.8$ , the perturbation is centered around  $r_0 = 4.8 M$  and has a width of  $\sigma = 1.0 M$ . We then compute the discrete Hamiltonian and momentum constraints  $\mathcal{H}$  and  $\mathcal{M}^i$  for these initial data sets, using the same (high) resolution, namely  $109 \times 109$  grid points on each block in the angular direction and 406 points in the radial direction, corresponding to  $\Delta r \approx 0.0148 M$ . Due to the symmetry of our six-block structure and the axisymmetry of the initial data, two components of the discrete momentum constraints coincide,  $\mathcal{M}^x = \mathcal{M}^y$ , and we therefore do not show the latter. The behavior of the constraints in the  $L_2$  and the  $L_\infty$  (not shown in the figure) norms agrees with eq. (35): for small amplitudes  $A$ , the discrete constraints at a fixed resolution appear to be independent of  $A$ , while for large amplitudes they show the expected quadratic dependence on  $A$ . We also show that the discrete constraint violations of our initial data sets have the expected dependence on resolution. For small amplitudes and coarse resolutions, the contribution of the quadratic term in eq. (35) is sufficiently small, so that the constraints seem to converge towards zero. However, for any given amplitude  $A$  a fine enough resolution  $h$  reveals that the convergence is actually towards a small but non-zero value, determined by the quadratic term in the expansion eq. (35). This behavior is shown in fig. 3. As an illustration we show there a convergence test for  $\mathcal{H}$  by comparing initial data for different resolutions. The highest resolutions are identical to those used in fig. 2. The other four resolutions shown are  $73 \times 73 \times 271$ ,  $49 \times 49 \times 181$ ,  $25 \times 25 \times 91$ , and  $17 \times 17 \times 61$  grid points per block, corresponding to  $\Delta r \approx 0.0222 M$ ,  $0.0333 M$ ,  $0.0667 M$ , and  $0.1 M$ , respectively.

#### IV. NUMERICAL STUDIES

##### A. Description of the simulations

We use the  $D_{8-4}$  operator constructed in [55], a summation by parts operator [67, 68] which is eighth order accurate in the interior and fourth order accurate at the boundaries, optimized to minimize its spectral radius and boundary truncation errors. Fifth order global convergence is expected [69, 70]. We integrate in time with a fourth order Runge–Kutta integrator with adaptive time stepping as described in [71].

In order to test both the long term stability and the convergence of our code, we first evolve a Kerr black hole in Kerr–Schild coordinates with spin  $j = 0.5$ . Fig. 4

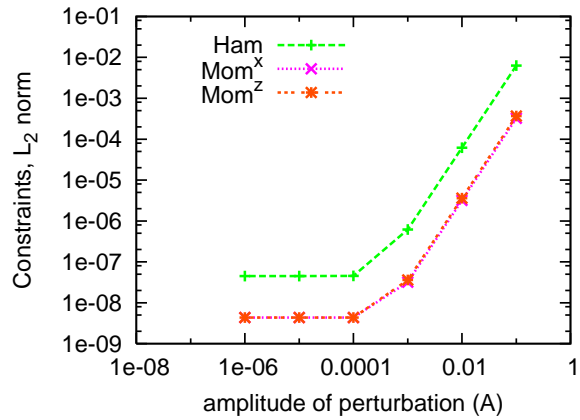


Figure 2: Discrete constraint violations for various perturbation amplitudes  $A$  at a fixed (high) resolution. We show the  $L_2$  norm for the Hamiltonian constraint and for two components ( $x$  and  $z$ ) of the momentum constraint (which turn out to be very close to each other, as the plot shows). The numerical resolution is  $109 \times 109$  grid points per block in the angular directions and  $\Delta r \approx 0.0148$  in the radial direction. The behavior is as expected and as described in the body of the paper: for sufficiently small amplitudes, the background contribution dominates the discretization error in the constraints, which then appear to be independent of  $A$ . For large enough amplitudes, the constraint violation has a quadratic dependence on  $A$  (with an exponent of  $2.01 \pm 0.01$  for the resolution shown in this figure), since for our initial data only the linearized constraints (around Schwarzschild) are satisfied.

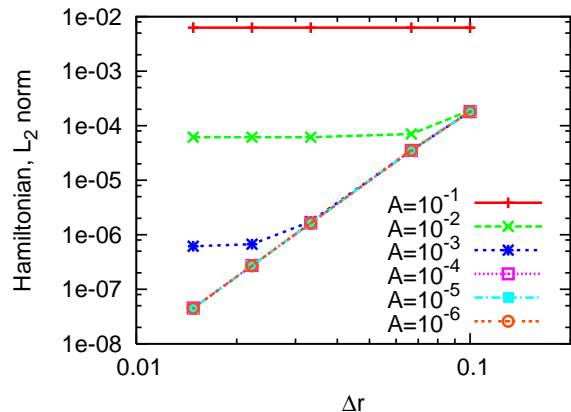


Figure 3:  $L_2$  norm of the Hamiltonian constraint for different amplitudes  $A$  of the perturbation and for different resolutions  $h$ . The coarsest resolution uses  $17 \times 17$  points per block in the angular directions and  $\Delta r = 0.1 M$  in the radial direction. We increase the resolution in all directions, up to  $109 \times 109$  points in the angular directions and  $\Delta r \approx 0.0148 M$  in the radial direction. Since only the linearized constraints are satisfied, the non-linear constraints do not converge to zero. For sufficiently large perturbation amplitudes and for sufficiently fine resolutions, the non-linear effects become visible, and the constraint violations converge to a constant value which depends on the amplitude  $A$ . As shown in the previous figure, this dependence is quadratic, as expected.



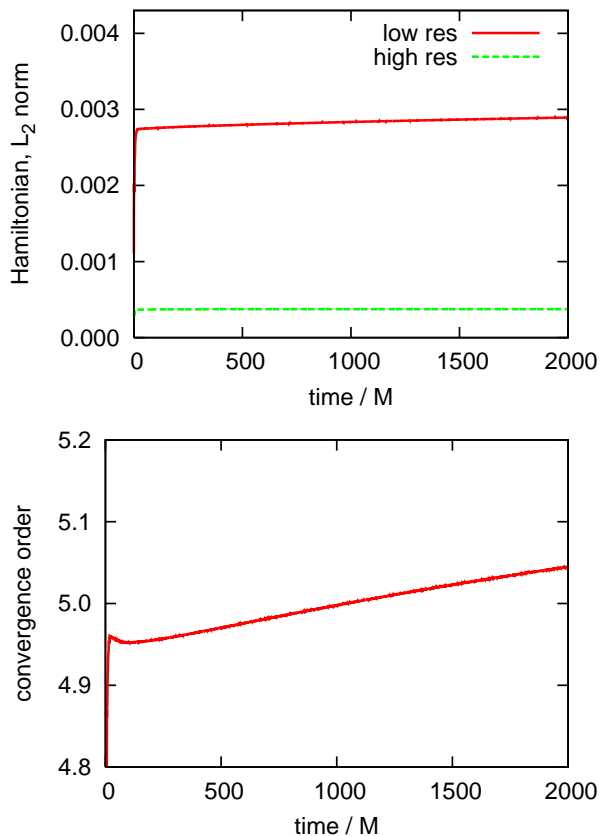


Figure 4:  $L_2$  norm (top panel) and convergence factor (bottom panel) for the Hamiltonian constraint for evolutions of a Kerr black hole with spin  $j = 0.5$ . The coarse resolution corresponds to  $16 \times 16$  points per block in the angular directions and  $\Delta r = 0.2 M$  in the radial direction. The fine resolution a factor of 1.5 higher in all directions. We see fifth order convergence, as expected for the difference operators used.

shows the  $L_2$  norm of the Hamiltonian constraint vs. time for two different resolutions. The radial domain extent is  $1.8 M < r < 11.8 M$ . The coarse resolution corresponds to  $\Delta r = 0.2 M$  and  $16 \times 16$  points per block in the angular directions, and the fine resolution increases the number of points in all directions by a factor of 1.5. We see approximate fifth order convergence, as expected.

In the simulations discussed below, we place our inner boundary at  $r = 1.8 M$  and our outer boundary at  $r = 251.8 M$ . This allows for observer locations up to  $r = 80 M$ , which are still causally disconnected from the outer boundary for times long enough to follow the ring-down, namely up to  $t = 280 M$ . We set up initial data according to eq. (34) with  $A = 0.01$ ,  $\sigma = 1.0 M$ , and  $r_0 = 20 M$ , where  $M$  is the mass of the black hole when the perturbation is switched off. Our coarse resolution uses  $16 \times 16$  points per block in the angular directions and 1251 points in the radial direction, corresponding to  $\Delta r = 0.2 M$ . Our fine resolution uses 1.4 times as many grid points in all directions.

One of the goals of the analysis that follows is to study the effect of the choice of the background metric on the accuracy of the waveforms. Since for this scattering problem solutions in closed form are not known, we compare the waves which we extract from our three-dimensional simulations to results obtained with an independent fourth order accurate one-dimensional code which solves the Regge–Wheeler equation (16). These 1D results were obtained with a resolution of  $\Delta r = 0.0125 M$ . The relative difference in this Regge–Wheeler function to a result from twice this resolution lies roughly between roundoff error and  $10^{-7}$ , which is far below the numerical errors that we expect from our 3D simulations. Therefore, we consider these 1D results in the following to be exact for all practical purposes.

### B. The standard and generalized RW approaches: numerical comparisons

We now analyze the results of evolving distorted black holes as described above and extracting gravitational waves with different methods.

Fig. 5 shows Regge–Wheeler functions for observers at  $r = 20 M$ ,  $40 M$ , and  $80 M$ , extracted with both our generalized approach and the standard one. The data have been scaled by a factor of 100 to normalize to an initial data amplitude  $A = 1$  in eq. (34). Recall that we used weak waves of amplitude  $A = 0.01$  for these simulations to avoid non-linear effects, and to be able to compare with the exact solution, which is only known in the linear regime.

Five waves are shown in fig. 5 for each observer location. Apart from the exact solution, we show two results obtained from our generalized approach, which coincide with each other in the continuum limit. They differ in how the background metric is computed: in one case we use the exact expressions for the Kerr–Schild background, and in the other case these coefficients were numerically calculated by extracting the  $\ell = 0$  part of the metric, as explained in sect. II B.

Finally, two waveforms were extracted using the standard approach with two different assumptions for the background, as found in the literature: a Minkowski spacetime in Minkowski coordinates, and a Schwarzschild spacetime in Schwarzschild coordinates. We want to highlight an interesting feature which can easily be seen in eq. (8). For any observer location, the waves extracted with these two background should differ only by a factor which is constant in time:

$$\Phi_{RW}^{\text{Min}} = \kappa \Phi_{RW}^{\text{Sch}}, \quad (36)$$

where  $\kappa^2 = g_{rr}^{\text{Sch}}$  is radial component of the Schwarzschild metric in Schwarzschild coordinates. Such a simple relationship is a direct consequence of the vanishing radial shift for these backgrounds. We confirmed this expected behavior numerically with high accuracy: at all times and

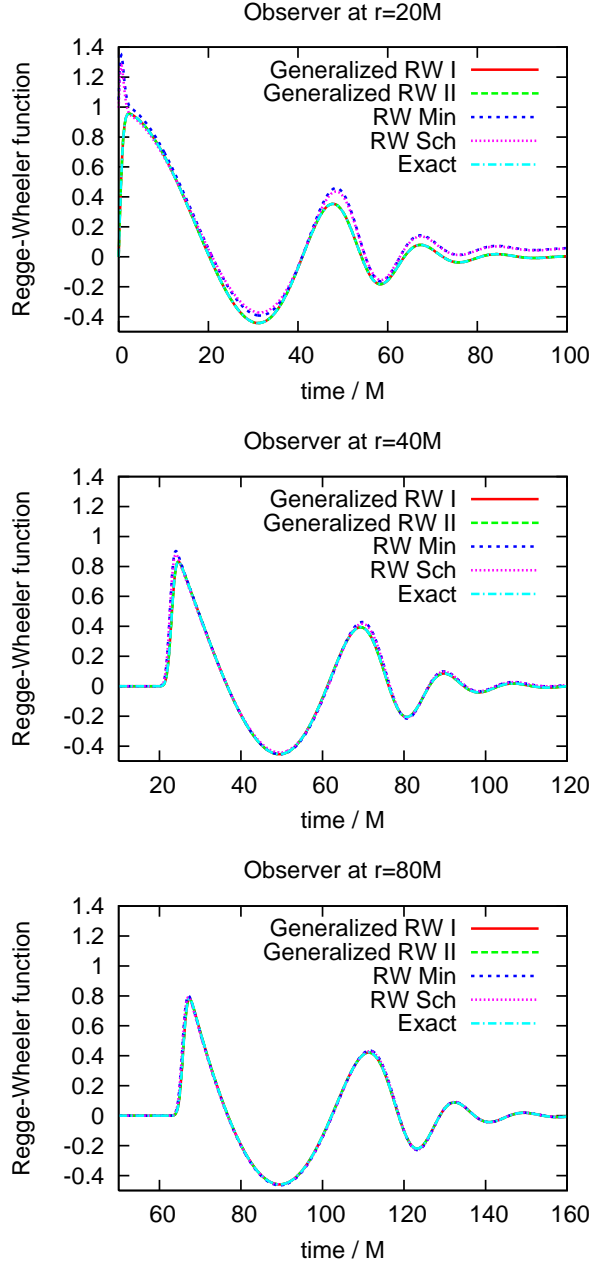


Figure 5: Extracted waveforms for observers at  $20M$ ,  $40M$ , and  $80M$ . Shown is the Regge–Wheeler function obtained from the standard RW approach and our generalized one. For the former we assumed both a Minkowski background and a Schwarzschild background in Schwarzschild coordinates, labeled as *RW Min* and *RW Sch*, respectively. For the generalized approach we show the results for two cases, in which the background metric is dynamically computed from the numerical solution (*Generalized RW I*), and where we prescribe it analytically (*Generalized RW II*). Also shown is the exact waveform. These simulations were performed with a resolution of  $16 \times 16$  grid points in the angular directions on each block and  $\Delta r = 0.2M$  in the radial direction. See the main text for more details.

for all observers we recover this expected ratio between the two waves to double precision roundoff error.

Figure 5 suggests that, as expected, the differences between waves extracted with different methods decrease as the extraction radius increases. At  $r = 80M$ , the curves show excellent agreement in the  $L_e$  norm<sup>4</sup>. For a more thorough comparison, we look at the differences between the extracted waves and the exact solution in fig. 6. For consistency with fig. 5, we also scaled the errors relative to the initial amplitude of the perturbation.

Perhaps the most notable feature in fig. 6 is that the differences between the waves obtained from generalized approach either with a numerically obtained background metric or with the exact (Kerr–Schild) background metric are smaller than the difference to the exact solution. For all practical purposes we can therefore consider them identical to each other, and for the rest of the paper we leave the latter out of the discussion.

Fig. 6 also shows that the standard approach—with either a Minkowski or Schwarzschild background—leads to errors which are considerably larger than the errors in our generalized approach, even for an observer at  $r = 80M$ . For the specific resolution that we used for fig. 6, the errors at  $r = 20M$  with the standard method are roughly three orders of magnitude larger than the errors with the generalized method. For  $r = 40M$  and  $80M$ , the ratio of the errors is of the order  $10^3$  to  $10^1$  and  $10^2$  to  $10^0$ , respectively.

The previous discussion only analyzes the errors introduced by the standard method at a fixed resolution. Next we discuss the dependence of these results on the resolution. It turns out that the difference between the different methods is even more striking for higher resolutions. By construction, the generalized wave extraction method should give the exact waveform in the continuum. At the discrete level, its associated errors should converge away with increasing resolution. Fig. 7 shows that this is actually the case. On the other hand, the errors in the standard approach do *not* converge to zero, as shown in fig. 7. In other words, the accuracy of the extracted waves with the standard method is dominated by the extraction procedure and not by the numerical resolution.

Fig. 7 as well as the second panel of fig. 6 show another interesting feature. Contrary to expectation, assuming Schwarzschild-like coordinates instead of a Minkowski background does not necessarily lead to smaller errors in the waveforms. For example, for an observer at  $r = 40M$  and during the time interval of about  $25M < t < 50M$ , the errors are actually up to one order of magnitude larger for the Schwarzschild-like coordinates. However, as can be seen from fig. 6, this feature depends on the observer location. We assume that this feature is only a coincidence.

<sup>4</sup> Also denoted by  $L_{\text{eyeball}}$

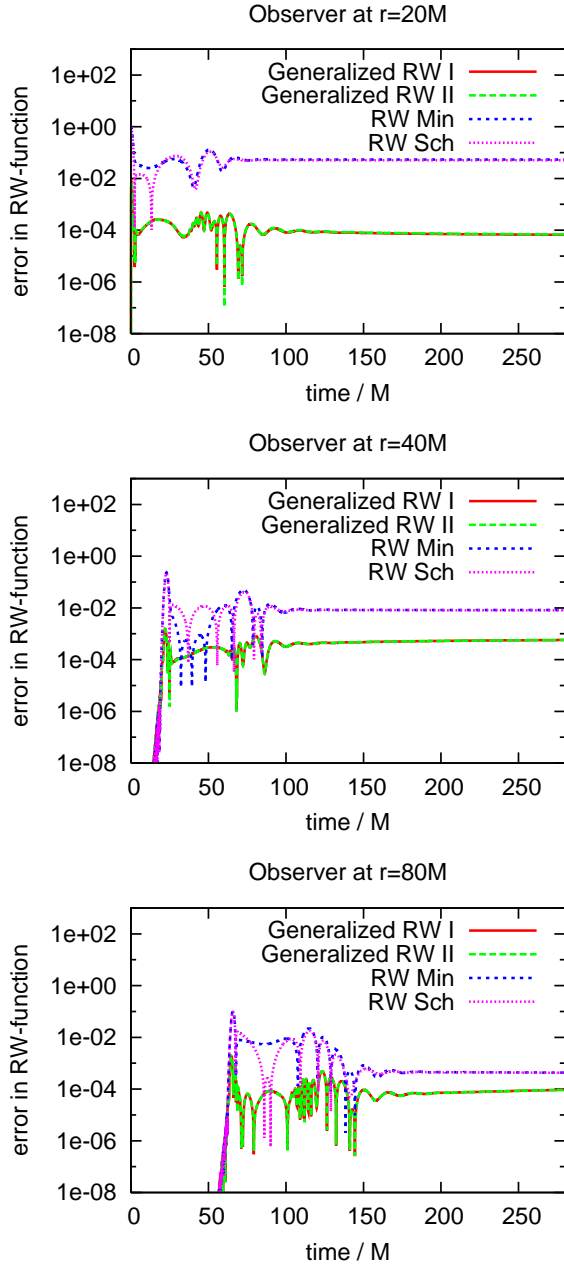


Figure 6: Errors for the waveforms shown in fig. 5.

The plateau in the errors seen in the last 100  $M$  to 200  $M$  in fig. 6 is due to an offset in the waveform. We found that, once the wave function decays to a small enough amplitude, it no longer oscillates around zero, but instead oscillates around a certain offset. This can be seen more clearly from the top panel in fig. 5. This offset is present for both the standard and the generalized extraction methods; however, there are important differences. The first is that the offset for the generalized extraction the offset converges to zero with increasing resolution, unlike for the standard method. The other is

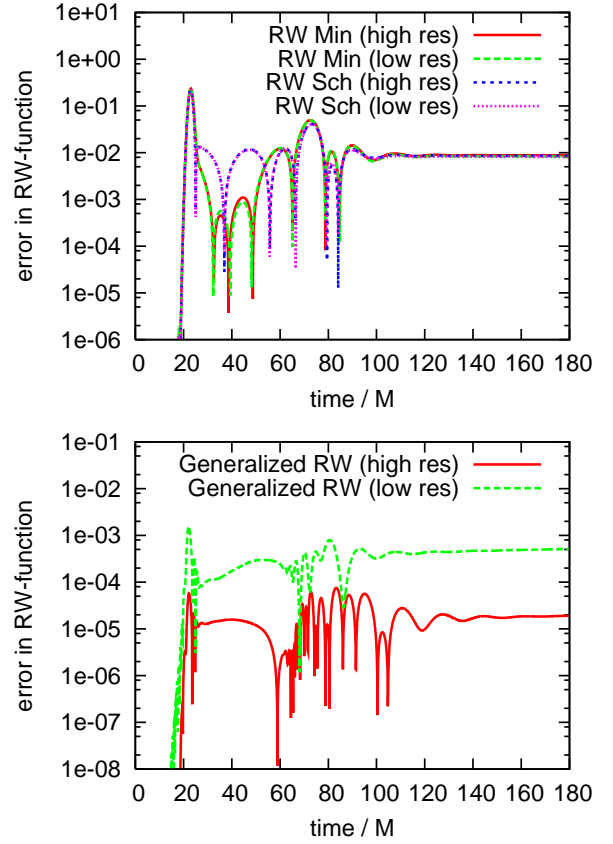


Figure 7: Shown is a convergence test for the simulations presented in the previous two figures. The plots labeled with “low res” coincide with the ones shown in the previous figures, while the plots labeled with “high res” correspond to 1.4 times that resolution. The error in the generalized wave extraction method, which by design gives the correct waveform in the continuum for these simulations, converges towards zero as expected. On the other hand, the errors in the standard wave extraction method are almost unaffected by the increased resolution. This indicates that these errors are dominated by the extraction method itself, not by the numerical truncation error. These results correspond to an observer at 40  $M$ , but they look similar for the other extraction radii that we consider in this paper.

that the offset for generalized method is orders of magnitude smaller than for the standard method. As we will discuss in the next subsection, that has direct consequences when attempting to extract quasinormal frequencies. This offset is reminiscent of the one that is present in RWZ waveforms when there is spin [72, 73].

The oscillatory feature of the wave can be followed for a longer time if the offset is subtracted from the waveform by hand, that is, if the wave is shifted along the vertical axis so that it oscillates around zero at late times. We do so by fitting the data to an exponentially decaying wave with an offset. (Details about the fit are given in the following subsection) The actual values that we de-

terminated for the offset are given in table I. As expected, the offset is decreasing with increasing radius for both standard RW wave extraction methods. This offset is mainly a result of the wrong assumption about the background metric, not of numerical error. There is no such clear dependence on the radius when using the new generalized extraction. Here the offset originates solely from truncation error, and converges to zero with increasing resolution. This behavior can also be seen in fig. 7.

Table I: Values of the offset for different wave extraction methods and observers at  $20M$ ,  $40M$  and  $80M$ .

Extraction Method	Observer	Offset
Generalized RW	$20M$	$-7.1 \times 10^{-5}$
Generalized RW	$40M$	$5.6 \times 10^{-4}$
Generalized RW	$80M$	$8.9 \times 10^{-5}$
RW Min	$20M$	$-5.4 \times 10^{-2}$
RW Min	$40M$	$-8.3 \times 10^{-3}$
RW Min	$80M$	$-4.4 \times 10^{-4}$
RW Sch	$20M$	$-5.1 \times 10^{-2}$
RW Sch	$40M$	$-8.1 \times 10^{-3}$
RW Sch	$80M$	$-4.3 \times 10^{-4}$

In fig. 8 we show the difference between the waveforms shifted by different offset values and the exact solution, for the same observers as before. As can be seen from the figure, our qualitative statements about the accuracies of the different wave extraction methods remain unchanged, if you consider the time span during which the amplitude of the wave is significant.<sup>5</sup> We conclude that the main errors in fig. 6 are *not* caused by an overall offset in the whole waveform.

### C. Quasinormal frequencies

We now turn our attention to extracting quasinormal frequencies from the waveforms just discussed. The primary goal is to find out whether these frequencies are affected by the choice of a specific wave extraction method, which may have some presumably small but non-vanishing systematic error for any finite extraction radius, and if so, by how much. We used data from the lower resolution run that we already analyzed in the previous section. The accuracy of the frequency does not change significantly if we use the higher resolution run instead.

The angular part of the initial data is a pure  $\ell = 2$ ,  $m = 0$  mode. Since the background has no angular

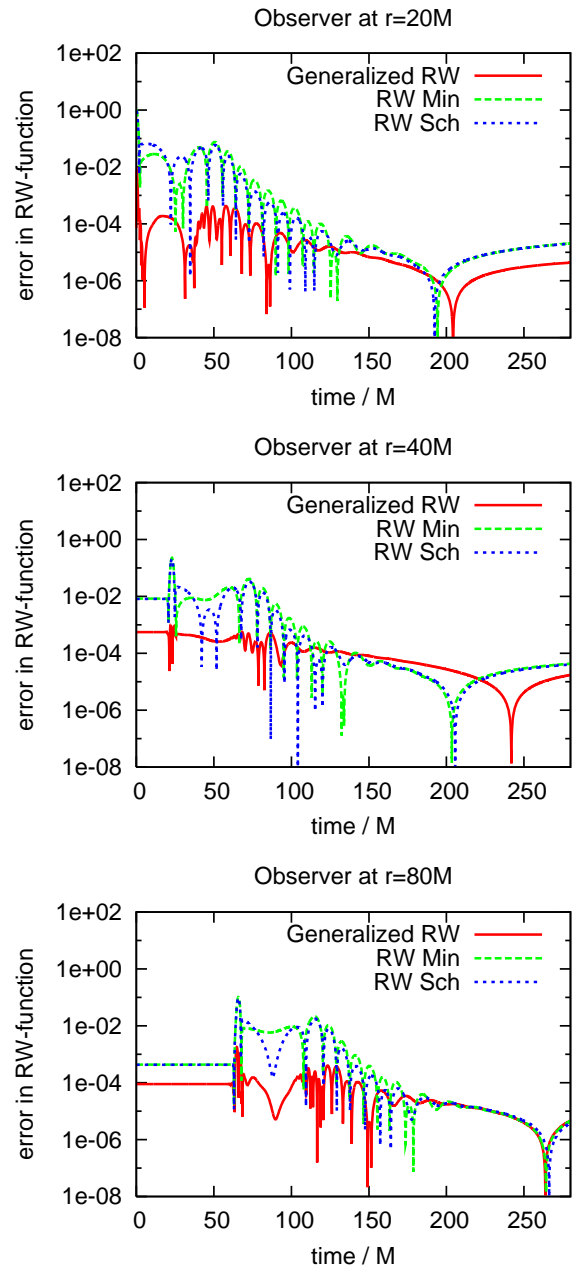


Figure 8: Shown are the same quantities as in fig. 6, except that an offset is subtracted from each waveform before calculating the errors. See the main text for details.

momentum, there is no mode-mode coupling at the linear level, while nonlinear coupling can be neglected for the current study, because we only evolve weak perturbations. Therefore the only dominant multipole mode present in the data at all times should be the one injected initially. At the numerical level,  $\ell = 4$  modes can be generated by our six-block grid structure. However, in [74] it was found that in the absence of angular momentum, these modes not only converge to zero with resolution,

<sup>5</sup> Of course, because we subtract the offset by hand to decrease the errors at late times, we can naturally follow the oscillatory part of the wave for longer times before.



but are also very small for the resolutions considered in this paper. In the above reference and in [75] it was also shown that overtones are not significantly excited unless the black hole is very rapidly rotating. Based on all this, we only fit for a single  $\ell = 2$ ,  $m = 0$  mode:

$$\Psi_{RW}^{fit} = \mathcal{A} \sin(\omega_r t + \chi) e^{i\omega_i(t-t_0)} - \xi \quad (37)$$

where  $\mathcal{A}$  is the excitation amplitude,  $\omega = \omega_r + i\omega_i$  is the complex quasinormal mode frequency,  $\chi$  is a phase shift,  $\xi$  is the offset and  $t_0$  is the starting time of the quasinormal ringing regime. The latter is not unambiguously defined (the so called “time-shift problem”), and as a consequence neither are the amplitudes of quasinormal modes. In ref. [74] it was proposed to minimize the uncertainties due to this time-shift problem by looking at carefully chosen relative amplitudes (see that reference for details). In order to fit numerical data to eq. (37), we fix  $t_0$  to an educated guess<sup>6</sup> and then fit for  $\omega$ ,  $\mathcal{A}$ ,  $\chi$ , and  $\xi$ . Any difference in  $t_0$  is absorbed in  $\mathcal{A}$  (in which we are not interested at this point) and does not change the other extracted parameters. We find the time-window of optimal fitting by looking for a local minimum in the relative residual between the original waveform and its fit. In ref. [74] it was found that such a local minimum is usually quite sharp and therefore gives a good criteria for choosing the window of time where the quasinormal ringing dominates. Similarly, we use the uncertainties in this minimum to quantify the errors in the parameters obtained in the fit. More details about the fitting procedure that we use to extract quasinormal parameters are given in ref. [74].

In the previous subsection we discussed the presence of an offset in the extracted waves with the standard method. If such an offset is not taken into account when fitting for the quasinormal frequencies (i.e., for a fixed  $\xi = 0$ ), eq. (37) does not represent the behavior of the numerical data well enough, and no reasonable results can be obtained from the fit. This is especially the case at medium to late time intervals when the amplitude becomes smaller than the offset, so that the wave does not cross zero any more. When one tries to fit for these cases, the obtained frequency has no relation at all to the correct QNM frequency. For example, at  $r = 20M$  the offset in the waves obtained from the standard RW wave extraction is of order  $10^{-2}$  for both a Minkowski background and for Schwarzschild-like coordinates. Without taking the offset into account, the value of  $\omega_r$  that the fit determines lies between  $10^{-14}$  and  $10^{-4}$ , and  $\omega_i$  is of order  $10^{-3}$  to  $10^{-6}$  (compare to table II). In contrast, the offset resulting from the generalized RW wave extraction is of order  $10^{-5}$  for this resolution. This is small enough that the problems described above do not play a noticeable role.

Table II shows the complex quasinormal frequencies that we obtained from the generalized and from the standard RW methods. As mentioned above and discussed in detail in ref. [74], the error bars are estimated from changes in the frequency when changing the time interval that we use for the fit of the waveform. We assume that the predicted frequency from perturbation theory for the fundamental  $\ell = 2$ ,  $m = 0$  mode is exact because we use a small amplitude for our perturbation. This frequency is known to be  $\omega_{\text{exact}} = 0.37367 - 0.08896i$  (see for example [76]). The frequency obtained from the new generalized wave extraction is consistent with this exact value within the accuracy to which we can obtain these numbers from the fit itself. For the standard wave extraction method, we only find agreement to three significant digits in the real part, but better agreement with the exact value in the imaginary part of the waveform. Note that, since the waveforms only differ by a constant factor (see subsec. IV B), the frequencies obtained with a Minkowski and a Schwarzschild background agree to roundoff error. The reason for the lower accuracy in the real part of  $\omega$  might be due to the fact that the waveforms are slightly distorted due to the wrong assumption for the background metric. This causes a larger residual between the data and the fit—it is about a factor of two larger than with the generalized wave extraction—and some degradation in how accurately certain fitting unknowns like  $\omega$  can be determined. That may also explain the larger relative error for the waves extracted with the standard RW wave method, which is shown in the right column of the same table. There the relative error is defined as  $|(\omega - \omega_{\text{exact}})/\omega_{\text{exact}}|$ .

## V. FINAL COMMENTS

When considering methods for extracting gravitational waves from numerical spacetimes at a finite distance, one question of direct interest is: How sensitive is the accuracy of the extracted waveforms to both the extraction method and observer location? In particular, how far away is “far enough” when extracting gravitational waves?

It is in general not easy to pose such a question in a precise way, since in order to quantify this one needs an exact waveform to compare with. This exact waveform is in principle only well defined at future null infinity. However, there are some particular scenarios of interest where the concept of “exact waveforms” at a finite distance can be given a well defined and precise sense. That is the case, for example, for perturbations of Kerr black holes (actually, of Petrov type  $D$  spacetimes): the Weyl scalar  $\Psi_4$  is defined everywhere in an essentially gauge and tetrad invariant way [77]. Similarly, for perturbations of Schwarzschild black holes, the Regge–Wheeler and Zerilli functions are defined in a gauge invariant way everywhere as well. In fact, there is a one-to-one mapping between these functions and  $\Psi_4$ ; see e.g. [15].

<sup>6</sup> For example, taking into account where the initial data and observer are located, and assuming a propagation speed of one

Table II: Quasinormal frequencies of the  $\ell = 2, m = 0$  mode as measured by an observer at  $r = 20M$ . Results are given for waveforms resulting from the different extraction methods we use. The predicted frequency from perturbation theory, which we assume to be exact because our perturbation amplitude is small, is  $\omega_{\text{exact}} = 0.37367 - 0.08896i$  [76]. The uncertainties in the extracted frequencies originate from variations in them depending on which interval of the waveform is used for the fit. The relative error is defined as  $|(\omega - \omega_{\text{exact}})/\omega_{\text{exact}}|$ .

Extraction Method	$\omega$	relative error
Generalized RW	$0.3736 - 0.0890i \pm (3 + 3i) \times 10^{-4}$	$1.9 \times 10^{-4} + 4.5 \times 10^{-4}i$
RW Min	$0.3733 - 0.0889i \pm (3 + 3i) \times 10^{-4}$	$9.9 \times 10^{-4} + 6.7 \times 10^{-4}i$
RW Sch	$0.3733 - 0.0889i \pm (3 + 3i) \times 10^{-4}$	$9.9 \times 10^{-4} + 6.7 \times 10^{-4}i$

Therefore the above question can be posed in a setting that might not be the most general one, but it is one in which a precise, quantitative answer can be found. The concrete setting that we chose for the current study is that of weak perturbations of Schwarzschild black holes. Furthermore, in this paper we restricted our treatment to odd parity perturbations (the even parity sector will be presented elsewhere). One of the standard methods that has been widely used for extracting gravitational waves from such spacetimes is through the standard Regge–Wheeler–Zerilli perturbation formalism. This formalism provides a gauge invariant treatment of perturbations of a background geometry defined by the Schwarzschild spacetime *in Schwarzschild coordinates*. That is, the formalism is invariant with respect to linear coordinate transformations *which leave the background coordinates fixed*. If one extracts waves using this formalism from a perturbation of Schwarzschild in, say, Kerr–Schild coordinates, the extracted waves at a finite distance will not be correct, even with if extracted with infinite numerical precision. There is a systematic error in such an extraction, due to the incorrect identification of the background coordinates. Of course, one expects this error to decrease as the extraction radius increases. In the spirit of the above discussion, the question that we asked ourselves was: how far away must the observer be, so that the difference between the exact waveform and the extracted one is negligible, if the extraction method has a systematic error? For this study we chose a very specific interpretation of “negligible systematic errors in the waveforms”, namely, that they are smaller than or comparable to the errors in these waveforms due to the numerical discretization.

In order to provide a quantitative answer to this question, in this paper we first proceeded to generalize the standard Regge–Wheeler extraction approach by using a perturbation formalism that allows for quite general slicing conditions for the Schwarzschild background. With this generalization, if one calculated with infinite resolution, one would extract the exact waveforms for *any* (not necessarily large) finite extraction radius. This holds even if the Schwarzschild background is, for example, given in a time dependent slicing, or one in which the coordinates in a neighborhood of the horizon are well

defined, as is usually the case in numerical black hole evolutions.

After summarizing the basics of the generalized formalism, we described our numerical implementation of the generalized extraction mechanism and our way of solving Einstein’s equations. For the latter we used multiple blocks and high order methods, both of which present several advantages. Of particular interest to this paper is that, due to the adaptivity that multiple blocks provide, the outer boundary can be placed at large distances, with much smaller computational costs than with Cartesian grids and mesh refinement. We made use of this specific advantage and performed three-dimensional non-linear simulations of weakly distorted Schwarzschild black holes, from which we extracted waves at distances larger than most current state-of-the-art three-dimensional simulations of Einstein’s equations.

Then we studied the dependence of the extracted waveforms on the extraction method. More precisely, we compared the standard RW method with our generalized one. We found that, even for the coarsest resolutions that we used, the errors in the waveforms from the standard method were dominated by the extraction procedure and not by the numerical accuracy of the spacetime metric. Furthermore, by increasing the resolution we could explicitly demonstrate that the errors in the standard method do not approach zero, while they do with the generalized one. While this is obviously the expected behavior on analytical grounds, we emphasize that we could explicitly see these differences even with an extraction radius which is significantly larger than those typically used in current state-of-the-art three-dimensional simulations.

What is not clear, however, is whether the wave zone resolution currently used by mesh refinement codes is sufficient to see the differences that we have demonstrated in this paper. For example, the spatial resolutions in the wave zone of current binary black hole inspiral and coalescence simulations are usually much coarser than the resolutions that we used above. Some radial resolutions  $h$  in the wave zone of binary black hole system simulations are: [78]  $h = 0.5M$ , [30]  $h = 0.5M$  (but the extraction is performed very close in at  $R = 16M$ ) [79]  $h = 0.75M$  (but  $h = 1.5M$  for calculating the radiated angular momentum  $J$ ), [80]  $h = 0.85M$ , [81]  $h = 0.87M$

[4]  $h = 0.82 M$ , [3]  $h = 0.56 M$ , [82]  $h = 0.56 M$ . Some of these codes are 4th order accurate, but many have at least certain components that are only 2nd order accurate.<sup>7</sup>

One of the interesting features of the waveforms that we extracted in this paper with the standard method is that we were able to “postprocess” them in order to remove an offset at late times. By doing so, we could accurately extract the quasinormal frequencies. However, we explicitly demonstrated that the large errors in the standard method were not due to an overall offset in the whole wave. Even after removing the offset “by hand”, errors of roughly the same order in the waves remained at early and intermediate times in the ringing regime. In addition, this postprocessing made use of the fact that we knew the qualitative behavior of the exact solution in the quasinormal ringing regime. In particular, we knew that it had to oscillate around zero, and we also knew what the frequencies they were supposed to have. It is not clear that one could apply such a postprocessing to decrease systematic errors in a more general scenario, where the characteristics of the expected waveforms are either completely unknown or not known with so much detail.

Concluding, in this paper we considered weak perturbations of Schwarzschild black holes, for which—as mentioned above—one can construct the Regge–Wheeler and Zerilli functions (or, equivalently,  $\Psi_4$ ) in an unambiguous way *everywhere*. In a more generic case (say, a collision of compact objects) this is not possible, and all gravitational wave extraction methods are inherently approximate at a fixed finite distance. The results of this paper suggest that, depending on the accuracy of a given simulation, different choices in the extraction procedure at a fixed and finite distance may result in relative differences in the waveforms that are actually larger than the numerical errors of the solution. These differences will in general decay with radius, but in a very slow way; typically as  $1/r$  (which is, in fact, the decay we found in our simulations). For example, in order to decrease the systematic errors for an observer at  $40 M$  shown in fig. 7 by, say, two orders of magnitude, by just moving the observer out and extracting at a single extraction radius, the latter would have to be located at  $\simeq 4,000 M$ . This means that, if similar uncertainties show up in other simulations for differing extraction methods, as the results of this paper suggest (and which can be tested), then decreasing those uncertainties by extracting waves at a *fixed* location and moving the observer further out does not seem

feasible, and other ideas would have to be explored.

## Acknowledgments

We thank Emanuele Berti, Steve Brandt, Barrett Deris, Luis Lehner, Jorge Pullin, Olivier Sarbach, and Saul Teukolsky for many helpful discussions and suggestions.

This research was supported in part by NSF grants PHY-0505761, PHY-0244699, PHY-0326311, PHY-0554793 and the National Center for Supercomputer Applications grant MCA02N014 to Louisiana State University. It also employed the resources of the Center for Computation & Technology at Louisiana State University, which is supported by funding from the Louisiana legislature’s Information Technology Initiative. AN thanks the CCT for an extended visit at Louisiana State University, where part of this work was done. MT thanks Saul Teukolsky for hospitality at Cornell University, and Reinaldo Gleiser and Oscar Reula for hospitality at FaMAF, where parts of this work were done. Our numerical calculations used the Cactus framework [62, 63] with a number of locally developed thorns, the LAPACK [83] and BLAS [84] libraries from the Netlib Repository [85], and the LAM [86, 87, 88] and MPICH [89, 90, 91] MPI [92] implementations.

---

<sup>7</sup> While it is currently common practice to report the finest resolution (near the horizons) and the coarsest resolution (near the outer boundary) in such simulations, the resolution in the wave zone, i.e., at the location where the gravitational waves are extracted, is often not explicitly listed, and can sometimes not be inferred. Some publications also do not report at which coordinate radius the wave information is extracted.

## Appendix A: VECTOR AND TENSOR SPHERICAL HARMONIC DECOMPOSITION (ODD AND EVEN-PARITY SECTORS)

We discuss now, in some detail, how to compute a multipole decomposition using vector and tensor spherical harmonics. A vector field  $V_A$  defined on the manifold  $S^2$  can be decomposed in multipoles using even and odd-parity basis vectors. Denoting the components in this basis by  $h_{\text{even}}^{(\ell,m)}$  and  $h_{\text{odd}}^{(\ell,m)}$ ,  $V_A$  can be written as

$$V_A = \sum_{\ell=1}^{\infty} \sum_{m=-\ell}^{\ell} h_{\text{even}}^{(\ell,m)} Y_A^{(\ell,m)} + h_{\text{odd}}^{(\ell,m)} S_A^{(\ell,m)}. \quad (\text{A1})$$

Here,  $Y_A^{(\ell,m)}$  and  $S_A^{(\ell,m)}$  are the even and odd-parity basis vectors tangent to the sphere, respectively. They are defined as

$$Y_A^{(\ell,m)} = \hat{\nabla}_A Y^{(\ell,m)} \quad (\text{A2})$$

$$S_A^{(\ell,m)} = \hat{\epsilon}_A^B \hat{\nabla}_B Y^{(\ell,m)}, \quad (\text{A3})$$

where  $\hat{\nabla}_A$  is the covariant derivative compatible with the unit sphere metric  $\hat{g}_{AB}$  and  $\hat{\epsilon}_{AB}$  is the Levi-Civita tensor with components  $\hat{\epsilon}_{\theta\phi} = \sin\theta$ . They satisfy the relations  $\hat{\nabla}_C \hat{g}_{AB} = 0$  and  $\hat{\nabla}_C \hat{\epsilon}_{AB} = 0$ . These vectors obey the orthogonality relations

$$\int \hat{g}^{AB} \bar{Y}_A^{(\ell,m)} Y_B^{(\ell',m')} d\Omega = \ell(\ell+1) \delta_{\ell\ell'} \delta_{mm'}, \quad (\text{A4})$$

$$\int \hat{g}^{AB} \bar{S}_A^{(\ell,m)} S_B^{(\ell',m')} d\Omega = \ell(\ell+1) \delta_{\ell\ell'} \delta_{mm'}, \quad (\text{A5})$$

$$\int \hat{g}^{AB} Y_A^{(\ell,m)} S_B^{(\ell',m')} d\Omega = 0. \quad (\text{A6})$$

Here  $d\Omega = \sin\theta d\theta d\phi$  is the area element in polar spherical coordinates and the bar denotes complex conjugation. Using the orthogonality property we can find the multipole modes  $h_{\text{even}}^{(\ell,m)}$  and  $h_{\text{odd}}^{(\ell,m)}$ . The result is

$$h_{\text{even}}^{(\ell,m)} = \frac{1}{\ell(\ell+1)} \int \hat{g}^{AB} V_A \bar{Y}_B^{(\ell,m)} d\Omega, \quad (\text{A7})$$

$$h_{\text{odd}}^{(\ell,m)} = \frac{1}{\ell(\ell+1)} \int \hat{g}^{AB} V_A \bar{S}_B^{(\ell,m)} d\Omega. \quad (\text{A8})$$

Using spherical coordinates the components of the even-parity basis are

$$Y_{\theta}^{(\ell,m)} = \partial_{\theta} Y^{(\ell,m)} \quad (\text{A9})$$

$$Y_{\phi}^{(\ell,m)} = \partial_{\phi} Y^{(\ell,m)}. \quad (\text{A10})$$

For the odd parity we get

$$S_{\theta}^{(\ell,m)} = -\frac{1}{\sin\theta} \partial_{\phi} Y^{(\ell,m)} \quad (\text{A11})$$

$$S_{\phi}^{(\ell,m)} = \sin\theta \partial_{\theta} Y^{(\ell,m)}. \quad (\text{A12})$$

Expanding the integral with these vector components we obtain that

$$h_{\text{even}}^{(\ell,m)} = \frac{1}{\ell(\ell+1)} \int V_{\theta} \bar{Y}_{\theta}^{(\ell,m)} + \frac{1}{\sin^2\theta} V_{\phi} \bar{Y}_{\phi}^{(\ell,m)} d\Omega, \quad (\text{A13})$$

$$h_{\text{odd}}^{(\ell,m)} = \frac{1}{\ell(\ell+1)} \int \frac{1}{\sin\theta} \left( V_{\phi} \bar{Y}_{\theta}^{(\ell,m)} - V_{\theta} \bar{Y}_{\phi}^{(\ell,m)} \right) d\Omega. \quad (\text{A14})$$

For tensors, the idea is the same. If  $V_{AB}$  is a tensor field defined on the unit sphere, the multipole decomposition takes the form

$$V_{AB} = \sum_{\ell=2}^{\infty} \sum_{m=-\ell}^{\ell} K^{(\ell,m)} \hat{g}_{AB} Y^{(\ell,m)} + G^{(\ell,m)} Y_{AB}^{(\ell,m)} + h_2^{(\ell,m)} S_{AB}^{(\ell,m)}, \quad (\text{A15})$$



where  $\hat{g}_{AB}Y^{(\ell,m)}$  and  $Y_{AB}^{(\ell,m)}$  are the even-parity tensor basis, whereas  $S_{AB}^{(\ell,m)}$  is the odd-parity tensor basis. We follow the Regge–Wheeler notation by using  $K$  and  $G$  for the even-parity components and  $h_2$  for the odd-parity one. The tensor basis is defined as

$$Y_{AB}^{(\ell,m)} = \hat{\nabla}_A \hat{\nabla}_B Y^{(\ell,m)} + \frac{1}{2}\ell(\ell+1)\hat{g}_{AB}Y^{(\ell,m)} \quad (\text{A16})$$

$$S_{AB}^{(\ell,m)} = \frac{1}{2}\left(\hat{\nabla}_A S_B^{(\ell,m)} + \hat{\nabla}_B S_A^{(\ell,m)}\right) \quad (\text{A17})$$

This definition agrees with Zerilli tensor harmonics up to a factor of 2, as we will see. They obey the orthogonality relations

$$\int \hat{g}^{AC} \hat{g}^{BD} \bar{Y}_{CD}^{(\ell,m)} Y_{AB}^{\ell'm'} d\Omega = \frac{1}{2}\ell(\ell-1)(\ell+1)(\ell+2)\delta_{\ell\ell'}\delta_{mm'}, \quad (\text{A18})$$

$$\int \hat{g}^{AC} \hat{g}^{BD} \bar{S}_{CD}^{(\ell,m)} S_{AB}^{\ell'm'} d\Omega = \frac{1}{2}\ell(\ell-1)(\ell+1)(\ell+2)\delta_{\ell\ell'}\delta_{mm'}, \quad (\text{A19})$$

and integration of the product of two different tensor basis vanishes. With this we can find  $K$ ,  $G$  and  $h_2$ . The result is

$$K^{(\ell,m)} = \frac{1}{2} \int V_{AB} g^{AB} \bar{Y}^{\ell m} d\Omega \quad (\text{A20})$$

$$G^{(\ell,m)} = \frac{2}{\ell(\ell-1)(\ell+1)(\ell+2)} \int \hat{g}^{AC} \hat{g}^{BD} V_{AB} \bar{Y}_{CD}^{(\ell,m)} d\Omega \quad (\text{A21})$$

$$h_2^{(\ell,m)} = \frac{2}{\ell(\ell-1)(\ell+1)(\ell+2)} \int \hat{g}^{AC} \hat{g}^{BD} V_{AB} \bar{S}_{CD}^{(\ell,m)} d\Omega \quad (\text{A22})$$

Using spherical coordinates the components of the basis are

$$Y_{\theta\theta}^{(\ell,m)} = \frac{1}{2}W^{(\ell,m)} \quad (\text{A23})$$

$$Y_{\theta\phi}^{(\ell,m)} = \frac{1}{2}X^{(\ell,m)} \quad (\text{A24})$$

$$Y_{\phi\phi}^{(\ell,m)} = -\frac{1}{2}\sin^2\theta W^{(\ell,m)} \quad (\text{A25})$$

$$S_{\theta\theta}^{(\ell,m)} = -\frac{1}{2\sin\theta}X^{(\ell,m)} \quad (\text{A26})$$

$$S_{\theta\phi}^{(\ell,m)} = \frac{1}{2}\sin\theta W^{(\ell,m)} \quad (\text{A27})$$

$$S_{\phi\phi}^{(\ell,m)} = \frac{1}{2}\sin\theta X^{(\ell,m)}, \quad (\text{A28})$$

where  $W^{(\ell,m)}$  and  $X^{(\ell,m)}$  are defined by Zerilli [93] as

$$W^{(\ell,m)} = 2\left[\partial_\theta^2 + \frac{1}{2}\ell(\ell+1)\right]Y^{(\ell,m)} \quad (\text{A29})$$

$$X^{(\ell,m)} = 2\partial_\phi(\partial_\theta - \cot\theta)Y^{(\ell,m)}. \quad (\text{A30})$$

Assuming that  $V_{AB}$  is a symmetric tensor and abbreviating the normalization constant as  $L = \ell(\ell-1)(\ell+1)(\ell+2)$ , we expand the integrals to get

$$K^{(\ell,m)} = \frac{1}{2} \int \left(V_{\theta\theta} + \frac{V_{\phi\phi}}{\sin^2\theta}\right) \bar{Y}^{(\ell,m)} d\Omega \quad (\text{A31})$$

$$G^{(\ell,m)} = \frac{1}{L} \int V_{\theta\theta} \bar{W}^{(\ell,m)} + \frac{1}{\sin^2\theta} \left(2V_{\theta\phi} \bar{X}^{(\ell,m)} - V_{\phi\phi} \bar{W}^{(\ell,m)}\right) d\Omega \quad (\text{A32})$$

$$h_2^{(\ell,m)} = \frac{1}{L} \int \frac{V_{\phi\phi}}{\sin^3\theta} \bar{X}^{(\ell,m)} + 2\frac{V_{\theta\phi}}{\sin\theta} \bar{W}^{(\ell,m)} - \frac{V_{\theta\theta}}{\sin\theta} \bar{X}^{(\ell,m)} d\Omega \quad (\text{A33})$$

The  $Y^{\ell m}$  are normalized with respect to the standard metric  $\hat{g}_{AB}$  on  $S^2$ , an exception being the cases  $\ell = 0$  and  $\ell = 1$ ; where we choose the normalization such that  $Y^{0,0} = 1$ , and  $\int_{S^2} Y^{1,m} \bar{Y}^{1,m} d\Omega = 4\pi/3$ .

- 
- [1] J. Winicour, *Living Rev. Relativity* **1**, 5 (1998), [Online article], URL <http://www.livingreviews.org/lrr-1998-5>.
- [2] P. Hübner, *Class. Quantum Grav.* **18**, 1871 (2001).
- [3] B. Brügmann et al. (2006), gr-qc/0610128.
- [4] A. Buonanno, G. B. Cook, and F. Pretorius (2006), gr-qc/0610122.
- [5] J. Baker, M. Campanelli, and C. O. Lousto, *Phys. Rev. D* **65**, 044001 (2002), gr-qc/0104063.
- [6] Y. Zlochower, J. G. Baker, M. Campanelli, and C. O. Lousto, *Phys. Rev. D* **72**, 024021 (2005), gr-qc/0505055.
- [7] D. R. Fiske, J. G. Baker, J. R. van Meter, D. Choi, and J. M. Centrella, *Phys. Rev. D* **71**, 104036 (2005), gr-qc/0503100.
- [8] H. Friedrich, *Class. Quantum Grav.* **13**, 1451 (1996).
- [9] M. Campanelli and C. O. Lousto, *Phys. Rev. D* **59**, 124022 (1999), gr-qc/9811019.
- [10] C. Beetle, M. Bruni, L. M. Burko, and A. Nerozzi, *Phys. Rev. D* **72**, 024013 (2005), gr-qc/0407012.
- [11] A. Nerozzi, C. Beetle, M. Bruni, L. M. Burko, and D. Pollney, *Phys. Rev. D* **72**, 024014 (2005), gr-qc/0407013.
- [12] L. M. Burko, T. W. Baumgarte, and C. Beetle, *Phys. Rev. D* **73**, 024002 (2006), gr-qc/0505028.
- [13] A. Nerozzi, M. Bruni, V. Re, and L. M. Burko, *Phys. Rev. D* **73**, 044020 (2006), gr-qc/0507068.
- [14] M. Campanelli, B. J. Kelly, and C. O. Lousto, *Phys. Rev. D* **73**, 064005 (2006), gr-qc/0510122.
- [15] O. Sarbach and M. Tiglio, *Phys. Rev. D* **64**, 084016 (2001), gr-qc/0104061.
- [16] T. Regge and J. Wheeler, *Phys. Rev.* **108**, 1063 (1957).
- [17] F. J. Zerilli, *Phys. Rev. Lett.* **24**, 737 (1970).
- [18] A. Abrahams and C. Evans, *Phys. Rev. D* **37**, 318 (1988).
- [19] A. Abrahams, in *Frontiers in Numerical Relativity*, edited by C. Evans, L. Finn, and D. Hobill (Cambridge University Press, Cambridge, England, 1989).
- [20] A. Abrahams and C. Evans, *Phys. Rev. D* **42**, 2585 (1990).
- [21] A. Abrahams and R. Price, *Phys. Rev. D* **53**, 163 (1996).
- [22] A. Nagar and L. Rezzolla, *Class. Quantum Grav.* **22**, R167 (2005), gr-qc/0502064.
- [23] K. Camarda and E. Seidel, *Phys. Rev. D* **57**, R3204 (1998), gr-qc/9709075.
- [24] K. Camarda and E. Seidel, *Phys. Rev. D* **59**, 064019 (1999), gr-qc/9805099.
- [25] S. Brandt, J. A. Font, J. M. Ibáñez, J. Massó, and E. Seidel, *Comp. Phys. Comm.* **124**, 169 (2000).
- [26] M. Alcubierre, G. Allen, B. Brügmann, G. Lanfermann, E. Seidel, W.-M. Suen, and M. Tobias, *Phys. Rev. D* **61**, 041501 (R) (2000), gr-qc/9904013.
- [27] J. Baker, S. R. Brandt, M. Campanelli, C. O. Lousto, E. Seidel, and R. Takahashi, *Phys. Rev. D* **62**, 127701 (2000), gr-qc/9911017.
- [28] M. Alcubierre, B. Brügmann, D. Pollney, E. Seidel, and R. Takahashi, *Phys. Rev. D* **64**, 061501(R) (2001), gr-qc/0104020.
- [29] M. Alcubierre, B. Brügmann, P. Diener, F. Herrmann, D. Pollney, E. Seidel, and R. Takahashi (2004), gr-qc/0411137.
- [30] F. Herrmann, D. Shoemaker, and P. Laguna (2006), gr-qc/0601026.
- [31] M. Shibata and K. Uryū, *Prog. Theor. Phys.* **107**, 265 (2002), gr-qc/0203037.
- [32] M. Shibata and Y.-i. Sekiguchi, *Phys. Rev. D* **71**, 024014 (2005), astro-ph/0412243.
- [33] M. D. Duez, S. L. Shapiro, and H.-J. Yo, *Phys. Rev. D* **69**, 104016 (2004), gr-qc/0401076.
- [34] U. Gerlach and U. Sengupta, *Phys. Rev. D* **19**, 2268 (1979).
- [35] K. Martel and E. Poisson, *Phys. Rev. D* **71**, 104003 (2005).
- [36] C. Gundlach and J. M. Martin-Garcia, *Phys. Rev. D* **61**, 08024 (2000), gr-qc/9906068.
- [37] L. Lindblom, M. A. Scheel, L. E. Kidder, R. Owen, and O. Rinne, *Class. Quantum Grav.* **23**, S447 (2006), gr-qc/0512093.
- [38] H. Friedrich, *Comm. Math. Phys.* **100**, 525 (1985).
- [39] O. Brodbeck, S. Frittelli, P. Hübner, and O. A. Reula, *J. Math. Phys.* **40**, 909 (1999), gr-qc/9809023.
- [40] C. Gundlach, J. M. Martin-Garcia, G. Calabrese, and I. Hinder, *Class. Quantum Grav.* **22**, 3767 (2005), gr-qc/0504114.
- [41] P. Secchi, *Differential Integral Equations* **9**, 671 (1996).
- [42] B. Brügmann, W. Tichy, and N. Jansen, *Phys. Rev. Lett.* **92**, 211101 (2004), gr-qc/0312112.
- [43] P. Diener, F. Herrmann, D. Pollney, E. Schnetter, E. Seidel, R. Takahashi, J. Thornburg, and J. Ventrella, *Phys. Rev. Lett.* **96**, 121101 (2006), gr-qc/0512108, URL <http://link.aps.org/abstract/PRL/v96/e121101>.
- [44] E. Schnetter, P. Diener, N. Dorband, and M. Tiglio, *Class. Quantum Grav.* **23**, S553 (2006), gr-qc/0602104, URL <http://stacks.iop.org/CQG/23/S553>.
- [45] M. A. Scheel, A. L. Erickcek, L. M. Burko, L. E. Kidder, H. P. Pfeiffer, and S. A. Teukolsky, *Phys. Rev. D* **69**, 104006 (2004), gr-qc/0305027.
- [46] L. E. Kidder, L. Lindblom, M. A. Scheel, L. T. Buchman, and H. P. Pfeiffer, *Phys. Rev. D* **71**, 064020 (2005), gr-qc/0412116.
- [47] M. A. Scheel, H. P. Pfeiffer, L. Lindblom, L. E. Kidder, O. Rinne, and S. A. Teukolsky (2006), gr-qc/0607056, gr-qc/0607056.
- [48] E.ourgoulhon, P. Grandclément, K. Taniguchi, J. Marck, and S. Bonazzola, *Phys. Rev. D* **63**, 064029 (2001).
- [49] P. Grandclément, E.ourgoulhon, and S. Bonazzola, *Phys. Rev. D* **65**, 044021 (2002), gr-qc/0106016.
- [50] H. P. Pfeiffer, L. E. Kidder, M. A. Scheel, and S. A. Teukolsky, *Comput. Phys. Commun.* **152**, 253 (2003), gr-qc/0202096.
- [51] M. Ansorg, B. Brügmann, and W. Tichy, *Phys. Rev. D* **70**, 064011 (2004), gr-qc/0404056.
- [52] M. Ansorg, *Phys. Rev. D* **72**, 024018 (2005), gr-qc/0505059.
- [53] F. Löffler, L. Rezzolla, and M. Ansorg, *Phys. Rev. D* **74**, 104018 (2006), gr-qc/0606104.
- [54] L. Lehner, O. Reula, and M. Tiglio, *Class. Quantum Grav.* **22** (2005), gr-qc/0507004.
- [55] P. Diener, E. N. Dorband, E. Schnetter, and M. Tiglio (2005), gr-qc/0512001, gr-qc/0512001.
- [56] M. Carpenter, D. Gottlieb, and S. Abarbanel, *J. Comput. Phys.* **111**, 220 (1994).
- [57] M. Carpenter, J. Nordström, and D. Gottlieb, *J. Com-*

- put. Phys. **148**, 341 (1999).
- [58] J. Nordström and M. Carpenter, J. Comput. Phys. **173**, 149 (2001).
  - [59] G. Calabrese, L. Lehner, D. Neilsen, J. Pullin, O. Reula, O. Sarbach, and M. Tiglio, Class. Quantum Grav. **20**, L245 (2003), gr-qc/0302072.
  - [60] G. Calabrese, L. Lehner, O. Reula, O. Sarbach, and M. Tiglio, Class. Quantum Grav. **21**, 5735 (2004), gr-qc/0308007.
  - [61] L. Lehner, D. Neilsen, O. Reula, and M. Tiglio, Class. Quantum Grav. **21**, 5819 (2004), gr-qc/0406116.
  - [62] T. Goodale, G. Allen, G. Lanfermann, J. Massó, T. Radke, E. Seidel, and J. Shalf, in *Vector and Parallel Processing – VECPAR’2002, 5th International Conference, Lecture Notes in Computer Science* (Springer, Berlin, 2003).
  - [63] Cactus Computational Toolkit home page, URL <http://www.cactuscode.org/>.
  - [64] E. Schnetter, S. H. Hawley, and I. Hawke, Class. Quantum Grav. **21**, 1465 (2004), gr-qc/0310042.
  - [65] Mesh Refinement with Carpet, URL <http://www.carpetcode.org/>.
  - [66] CactusEinstein Toolkit home page, URL <http://www.cactuscode.org/Community/NumericalRelativity/>.
  - [67] H. O. Kreiss and G. Scherer, in *Mathematical Aspects of Finite Elements in Partial Differential Equations*, edited by C. D. Boor (Academica Press, New York, 1974).
  - [68] H. O. Kreiss and G. Scherer, Tech. Rep., Dept. of Scientific Computing, Uppsala University (1977).
  - [69] B. Gustafsson, Tech. Rep. 33, Department of Computer Science, Uppsala University (1971).
  - [70] B. Gustafsson, Mathematics of Computation **29**, 396 (1975).
  - [71] W. H. Press, B. P. Flannery, S. A. Teukolsky, and W. T. Vetterling, *Numerical Recipes* (Cambridge University Press, Cambridge, England, 1986), URL <http://www.nr.com/>.
  - [72] M. Alcubierre, W. Bengert, B. Brügmann, G. Lanfermann, L. Nierger, E. Seidel, and R. Takahashi, Phys. Rev. Lett. **87**, 271103 (2001), gr-qc/0012079.
  - [73] S. Brandt and E. Seidel, Phys. Rev. D **52**, 870 (1995), URL <http://link.aps.org/abstract/PRD/v52/p870>.
  - [74] E. N. Dorband, E. Berti, P. Diener, E. Schnetter, and M. Tiglio, Phys. Rev. D **74**, 084028 (2006), gr-qc/0608091.
  - [75] E. Berti and V. Cardoso (2006), gr-qc/0605118.
  - [76] E. Leaver, Proc. R. Soc. London, Ser. A **402**, 285 (1985).
  - [77] S. Chandrasekhar, *The Mathematical Theory of Black Holes* (Oxford University Press, Oxford, England, 1983).
  - [78] J. G. Baker, J. Centrella, D.-I. Choi, M. Koppitz, and J. van Meter, Phys. Rev. Lett. **96**, 111102 (2006), gr-qc/0511103.
  - [79] J. G. Baker, J. Centrella, D.-I. Choi, M. Koppitz, and J. van Meter, Phys. Rev. D **73**, 104002 (2006), gr-qc/0602026.
  - [80] F. Pretorius, Class. Quantum Grav. **23**, S529 (2006), gr-qc/0602115.
  - [81] U. Sperhake (2006), gr-qc/0606079.
  - [82] J. A. Gonzáles, U. Sperhake, B. Brügmann, M. Hannam, and S. Husa (2006), gr-qc/0610154.
  - [83] LAPACK: Linear Algebra Package, URL <http://www.netlib.org/lapack/>.
  - [84] BLAS: Basic Linear Algebra Subroutines, URL <http://www.netlib.org/blas/>.
  - [85] Netlib Repository, URL <http://www.netlib.org/>.
  - [86] G. Burns, R. Daoud, and J. Vaigl, in *Proceedings of Supercomputing Symposium* (1994), pp. 379–386, URL <http://www.lam-mpi.org/download/files/lam-papers.tar.gz>.
  - [87] J. M. Squyres and A. Lumsdaine, in *Proceedings, 10th European PVM/MPI Users’ Group Meeting* (Springer-Verlag, Venice, Italy, 2003), no. 2840 in Lecture Notes in Computer Science, pp. 379–387.
  - [88] LAM: LAM/MPI Parallel Computing, URL <http://www.lam-mpi.org/>.
  - [89] W. Gropp, E. Lusk, N. Doss, and A. Skjellum, Parallel Computing **22**, 789 (1996).
  - [90] W. D. Gropp and E. Lusk, *User’s Guide for mpich, a Portable Implementation of MPI*, Mathematics and Computer Science Division, Argonne National Laboratory (1996), ANL-96/6.
  - [91] MPICH: ANL/MSU MPI implementation, URL <http://www-unix.mcs.anl.gov/mpi/mpich/>.
  - [92] MPI: Message Passing Interface Forum, URL <http://www.mpi-forum.org/>.
  - [93] F. J. Zerilli, J. Math. Phys. **11**, 2203 (1970).